Journal of Applied Fluid Mechanics, Vol. 17, No. 12, pp. 2807-2818, 2024.
Available online at www.jafmonline.net, ISSN 1735-3572, EISSN 1735-3645.
https://doi.org/10.47176/jafm.17.12.2645

Effect of Exhaust Jet from Takeoff Aircraft on the Inlet Distortion of Runway-Crossing Aircraft

X. Sun[1], W. Cheng[1], Y. Fu[1], X. He[2], Y. Chen[2], and S. Ma[3†]

[1] *Country College of Aviation Engineering, Civil Aviation Flight University of China, Guanghan, 618307, China*
[2] *Country Civil Aviation Flight Technology and Flight Safety Research Base, Civil Aviation Flight University of China, Guanghan, 618307, China*
[3] *College of Flight Technology, Civil Aviation Flight University of China, Guanghan, 618307, China*

†*Corresponding Author Email: shannirvana@cafuc.edu.cn*

ABSTRACT

Runway crossing behind an aircraft has attracted a large amount of interest in recent years. In this work, based on a turbofan engine model, three-dimensional models of the nozzle and inlet are established, and the effects of the jet of the aircraft in front on the inlet of the aircraft behind are studied under different operating conditions using numerical simulations. The results show that at the same distance between the two aircraft, the total pressure decreases as the exit flow rate of the inlet increases, but different flow rates do not lead to different component distributions. For the same flow rate at the exit of the inlet, when the distance increases, the distortion index of the total pressure at the exit of the inlet decreases, and the contents of the component of the airflow entering the inlet from the jet decrease, but those entering the inlet from the far field increase. Through component and isotope identification, the main components of the airflow entering the inlet are oxygen and nitrogen. Based on these results, when studying the effect of the exhaust jet from an aircraft on an aircraft behind, only the maximum idle engine speed needs to be considered, and the effect of the jet components on the inlet can be ignored. The inlet distortion caused by the exhaust flow is more severe in crosswind environments.

Article History

Received February 13, 2024
Revised June 5, 2024
Accepted June 16, 2024
Available online October 2, 2024

Keywords:

Runway-crossing
Numerical simulation
Jet effect
Inlet distortion
Component and isotope identification

1. INTRODUCTION

Simultaneous multi-runway operation allows for increased throughput of an airport, relieves pressure, improves the efficiency of airport operation, and ensures an on-time performance rate (Lu & Yu, 2011; Ren & Wang, 2015). Runway crossings arise from a multi-runway operation mode. Currently, the two main ways to cross a runway are as follows: (1) crossing in front of the takeoff aircraft, which requires the crossing aircraft to wait at the crossing until the takeoff aircraft flies abeam and makes runway incursion more likely to occur; (2) the "Big U-tax" method, in which the crossing aircraft needs to taxi around the end of the runway to the other side of the runway (ICAO, 2010; Chen et al., 2019). Both these runway-crossing modes increase the taxi waiting time and may not fully utilize the operating efficiency of the multi-runway mode. However, the method of crossing a runway behind the takeoff aircraft (i.e., rear-side crossing) was proposed in some studies. This method not only avoids conflicts but also ensures the operating efficiency of the multi-runway mode. This is an efficient, safe way to cross a runway, so it has attracted great attention in recent years (He & Zhang, 2019).

In the rear-side crossing mode, the landing aircraft crosses the runway after taxing along the taxiway to a safe distance behind a takeoff aircraft with the permission and guidance of the airport controller. Presently, Chicago O'Hare International Airport in the United States adopts this runway-crossing method, as shown in Fig. 1, and the airport operates well (Chen et al., 2021). However, owing to safety considerations, no relevant civil-aviation organization standards exist for this runway-crossing mode. This is because in this crossing mode, the jet from the takeoff aircraft may have serious consequences, such as a deviation from the taxiing route and the rollover of the aircraft crossing the runway, so additional attention is warranted (Zhang et al., 2016). In China, some studies have been done on this subject. Using Chongqing Jiang-bei Airport as a study case, Chen et al. (2018) analyzed the takeoff performance, jet effective distance, and taxi crosswind-resistance standard of typical aircraft at the airport. They

NOMENCLATURE

$\bar{D}$	distortion index	p^*_{max}	maximum total pressure at the exit of the inlet
f	molar composition	p^*_{min}	minimum total pressure at the exit of the inlet
$\dot{m}$	mass flow at the exit of the inlet	$\overline{p^*}$	mass-weighted average of the total pressure at the exit of the inlet
P_b^*	total pressure at the bypass entrance of the nozzle	T_b^*	total temperature at the bypass entrance of the nozzle
P_c^*	total pressure at the core entrance of the nozzle	T_c^*	total temperature at the core entrance of the nozzle
P_0^*	total pressure at the far-field entrance of the nozzle	T_0^*	total temperature at the far-field entrance of the nozzle
P_b	atmospheric pressure		

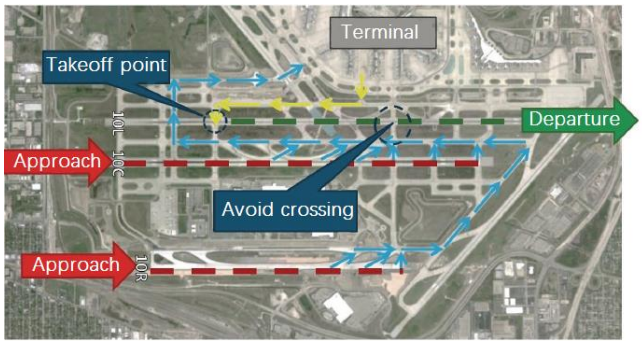

Fig. 1 The method of crossing the runway behind the takeoff point used at O'Hare Airport

preliminarily verified that the rear-side crossing mode could greatly improve the efficiency while ensuring the safety of a multi-runway operation. Zhang (2019) used a genetic algorithm to optimize taxiing paths for different runway-crossing modes. The results show that the rear-side crossing mode could shorten the total ground taxiing time of an aircraft and improve the efficiency of the airport surface operation. He et al. (2020) and Zhang (2021) constructed mathematical models for front-side crossing and rear-side crossing modes, and they compared the ground taxiing time of these two modes using a genetic algorithm. The results show that the combined use of the front-side and rear-side crossing modes could improve the surface taxiing efficiency when the front crossing delay was large. Furthermore, He et al. (2020) and Hu (2020) used numerical simulation methods to study the three-dimensional flow field of an aero-engine nozzle and the crosswind resistance of a rear-side crossing aircraft during the taxiing phase, and they determined the safe distance to the takeoff aircraft. He et al. (2021) constructed a crosswind-resistance model for an aircraft in the low-speed taxiing phase. Then, five typical aircraft types at Chongqing Jiang-bei Airport were used to verify the model. The results show that it can quickly and accurately calculate the wind-resistance capacity of different aircraft types. Chen et al. (2021) proposed a runway-crossing conflict-resolution model for the front-side and rear-side crossing modes. The rear-side crossing mode was verified. The impact of the distance between the two aircraft on the runway-crossing aircraft was studied by Guo (2023). A reference basis for the rear-side crossing mode was provided. The taxiing stability of an aircraft crossing a runway behind the takeoff point of another aircraft was studied by Wang (2023). For the cases of B737-800 being the takeoff aircraft and B737-800 and A320 being the rear aircraft crossing the runway, the taxiing stability of the rear aircraft under different distances between the two aircraft were studied, and a safe distance was recommended.

Based on the literature, it can be seen that the key problem to be solved for the rear-side crossing mode is whether the exhaust jet from the takeoff aircraft seriously affects the aircraft crossing the runway. In China, the research has mainly focused on the crossing aircraft's ability to resist crosswinds because the crossing aircraft faces strong crosswinds. However, the engine of the crossing aircraft also faces strong crosswinds at the same moment and is in an idle state. It is well known that when an engine is running in an idle state, the compressor is prone to surging, and the engine is unstable. A strong crosswind is more likely to cause inlet distortion, causing a compressor surge; in addition, the engine jet from the takeoff aircraft may also enter the engine of the runway-crossing aircraft, and the exhaust gas in the jet may cause further inlet distortion and a compressor surge. Therefore, in this crossing mode, attention should also be paid to the effects of the engine jet from the takeoff aircraft on the engine inlet of the runway-crossing aircraft. However, few relevant studies have been published on this topic. Inlet distortion and its effect on compressor stability have been studied in other countries. Since 1978, the S-16 Technical Committee of the United States has issued several guidelines for inlet-distortion assessments, such as ARD-50015 (SAE 1991) and AIR-1419d (SAE 2023), and it has standardized the experimental design and experimental evaluation processes in research on inlet distortion. These guidelines have rapidly developed into common standards in the United States and Europe. Thomas & Leonhard (2002) experimentally studied the effects of inlet distortion on high-pressure compressors. The results show that when the design speeds were 50% and 60%, the co-rotating inlet distortion caused a loss of surge margin of up to 90%. Moreover, an experimental study by Donald & Matt (2005) showed that the introduction of low inlet distortion at the rotor tip led to stage stalls in low-aspect-ratio military fans. An experimental study by Jiang et al. (2009) showed that inlet distortion seriously reduced the compressor efficiency, total-pressure-recovery coefficient, and stall margin. Yan et al. (2014) concluded from experiments that the inlet distortion had

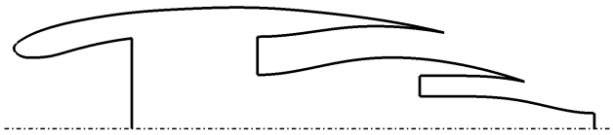

Fig. 2 Profile of a turbofan engine

a certain effect on the stall limit of a compressor. The experimental results of Ross et al. (2018) show that for a smooth inlet transonic axial flow compressor performance, when the total inlet pressure distortion degree was less than 90 degrees, the compressor efficiency peak distortion was less than 3%. It can be determined that inlet distortion has an important effect on compressor stability. Therefore, this paper discusses the effects of the jet from a takeoff aircraft on the inlet distortion of an aircraft crossing the runway behind the takeoff aircraft.

In this work, based on a turbofan engine configuration, three-dimensional models of the exhaust nozzle of the aircraft in front and the inlet of the aircraft behind were established, and the effects of the exhaust jet on the inlet with a numerical simulation method were calculated. During the numerical calculation, to reduce the amount of calculation and save calculation time, the numerical simulation was performed with a multistep calculation. The airflow entering the engine inlet of the aircraft may come from the core nozzle, bypass nozzle, or even far field of the nozzle of the aircraft in front. Therefore, to quantitatively evaluate the proportion of each part of the airflow in the inlet, especially the proportion of exhaust gas, component and isotope identification was used to set the gas components of each boundary condition based on the real engine operating conditions.

2. CALCULATION METHOD

2.1 Calculation Model

To simulate the effects of a jet from the takeoff aircraft on the engine inlet of an aircraft crossing the runway after the takeoff point, it is necessary to establish the calculation model of the nozzle and the inlet. In this research, based on the configuration of a turbofan engine shown in Fig. 2, the three-dimensional model of the inlet was generated by rotating the nacelle shape line and the inlet shape line around the symmetry axis once, as shown in Fig. 3 (a). The three-dimensional model of the nozzle was generated by rotating the mold line of the rear half of the nacelle and the exhaust system (including the bypass nozzle, core nozzle, and tail cone) around the symmetry axis, as shown in Fig. 3 (b). In the established models, the diameters of the outlet of the bypass nozzle, the core nozzle, and the inlet were 1,487.2 mm, 729.5 mm, and 1,401 mm, respectively.

The established nozzle and inlet models were arranged according to the layout shown in Fig. 4 to simulate runway-crossing aircraft. The aircraft that is taking off is represented by the nozzle arranged horizontally, and the runway-crossing aircraft is

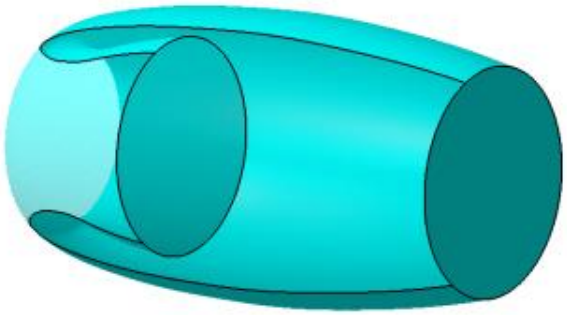

(a) Inlet model

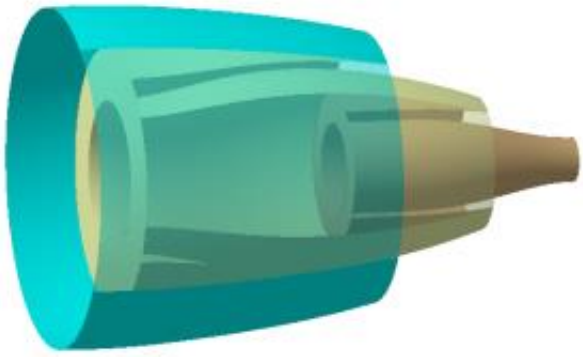

(b) Exhaust nozzle model

Fig. 3 Calculation models of inlet and exhaust nozzle

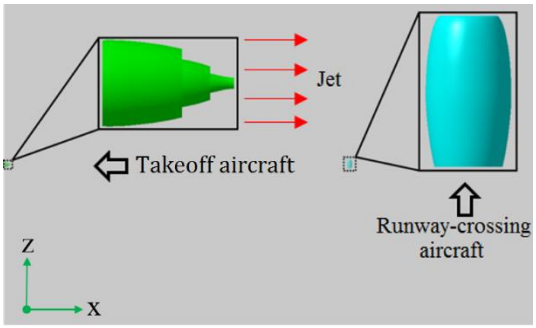

Fig. 4 Simulations of nozzle and inlet in the mode of crossing the runway behind the takeoff point

represented by the inlet arranged vertically. The inlet model is located on the axis of the nozzle. With this layout, the computational model is symmetrical about the y=0 plane.

2.2 Numerical Method

ANSYS CFX software was used to simulate the flow field of the nozzle and inlet. The three-dimensional, steady, compressible Reynolds-averaged Navier-Stokes equations were numerically solved. The governing equations are shown as follows:

$$\frac{\partial}{\partial x_i}(\overline{\rho}\overline{u_i} + \overline{\rho' u_i'}) = 0 \tag{1}$$

$$\frac{\partial}{\partial t}(\overline{\rho}\overline{u_i}+\overline{\rho' u_i'})+\frac{\partial}{\partial x_j}(\overline{\rho}\overline{u_i}\overline{u_j})=\overline{\rho}\overline{f_i}-\frac{\partial \overline{p}}{\partial x_i}+\mu\nabla^2\overline{u_i}+\frac{\mu}{3}\frac{\partial^2\overline{u_j}}{\partial x_i\partial x_j}+\frac{\partial}{\partial x_j}(-\overline{\rho}\overline{u_i'u_j'}-\overline{u_j}\overline{\rho' u_i'}-\overline{u_i}\overline{\rho' u_j'}-\overline{\rho' u_i'u_j'}) \quad (2)$$

$$\overline{\rho}\frac{D}{Dt}(\overline{e}+\frac{1}{2}\overline{u_i}^2)=\overline{\rho}\overline{u_i}\overline{f_i}+\frac{\partial}{\partial x_i}(k\frac{\partial \overline{T}}{\partial x_i})-\frac{\partial}{\partial x_i}(\overline{p}\overline{u_i})+\frac{\partial}{\partial x_j}(\overline{m_{ji}}\overline{u_i})+\overline{f_i}\overline{\rho' u_i'}-\frac{\partial}{\partial x_i}(\overline{p' u_i'})+\frac{\partial}{\partial x_j}(\overline{m_{ji}' u_i'})-\overline{\rho'\frac{De'}{Dt}}-\overline{\rho}\frac{D}{Dt}(\frac{1}{2}\overline{u_i'u_i'})-\overline{\rho'\frac{D}{Dt}(\frac{1}{2}u_i'u_i')} \quad (3)$$

where m_{ij} represents Newtonian viscous stress, and its expression is as follows:

$$m_{ij}=\begin{cases}\mu(\frac{\partial u_i}{\partial x_j}+\frac{\partial u_j}{\partial x_i}),(i\neq j)\\ 2\mu\frac{\partial u_i}{\partial x_i}-\frac{2}{3}\mu div(\vec{u}),(i=j)\end{cases} \quad (4)$$

The expression of the Reynolds stress is as follows:

$$-\rho\overline{u_i'u_j'}=\mu_t\left(\frac{\partial u_i}{\partial x_j}+\frac{\partial u_j}{\partial x_i}\right)-\frac{2}{3}\rho k\delta_{ij} \quad (5)$$

where μ_t represents the eddy viscosity coefficient, and its value is determined by the turbulence model.

The heat-transfer model is a total-energy model suitable for high-speed flow and compressible flow that considers the heat conduction caused by fluid kinetic energy. Both the convective terms in the momentum equation and in the turbulent transport equation are in a high-precision format. The turbulence model is the shear stress transport (SST) κ-ω turbulence model. The reason for using this model is that there is flow separation inside the inlet, and the κ-ω model based on SST was designed to give highly accurate predictions of the onset and the amount of flow separation under adverse pressure gradients. The model achieves this by the inclusion of transport effects into the formulation of the eddy-viscosity.

In the process of numerical calculation, to reduce the amount of calculation and save calculation time, the numerical simulation was carried out with a multistep calculation. First, the flow field of the nozzle was numerically calculated. Then, the aerodynamic parameters were assigned to the entrance boundary of the inlet. Finally, the flow field of the inlet was numerically calculated. In this calculation method, ICEM software was used for meshing of the nozzle and its far-field domain, along with the inlet and its far-field domain. The meshes are shown in Fig. 5. The meshes of the inner flow paths of the nozzle and the inlet used O-shaped elements. The near-wall meshes of the nozzle and the inlet were densified so that $y^+<1$. The field area was a rectangle of 60 m*200 m. The far-field area of the air inlet was a rectangle of 60 m*300 m.

Figure 6 shows the boundary condition settings of the nozzle and the inlet calculation models. The core and bypass nozzle entrances and their far-field entrance were set as the pressure entrance boundary, of which the total

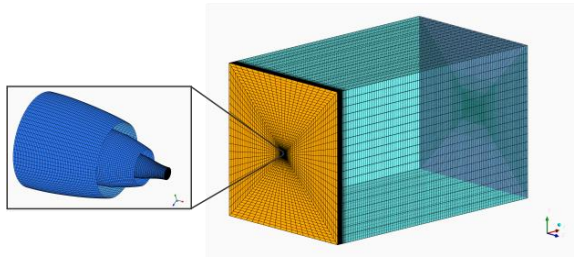

(a) Exhaust nozzle and its far field

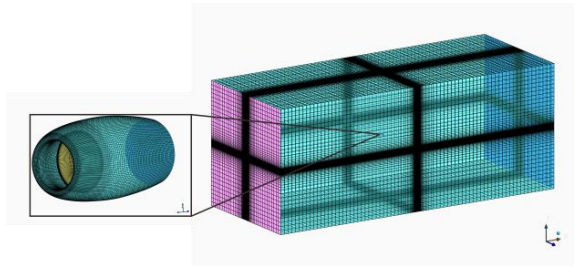

(b) Inlet and its far field

Fig. 5 Meshes used in the calculation

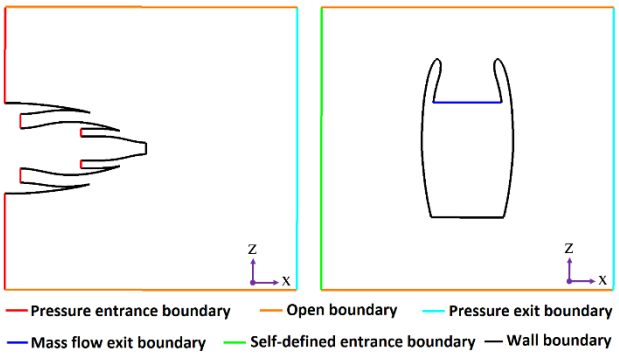

Fig. 6 Boundary conditions of the calculation model

pressure, total temperature, and flow angle were prescribed. The far-field entrance of the inlet was set as a self-defined entrance boundary, in which the velocity in three coordinate directions, static pressure, and static temperature were provided. The far-field exit of the nozzle and the far-field exit of the inlet were set as the pressure exit boundaries, in which the static pressure was imposed. The other far-field parts of the two were set as open boundaries, in which static pressure and static temperature were given. The exit of the inlet was set as the mass flow exit boundary, in which the value of the mass flow rate was provided. The rest of the nozzle and the inlet were set as the impermeable, non-slipped, and adiabatic wall boundary.

The core, bypass, and far-field airflow of the nozzle of the takeoff aircraft could enter the air inlet of the runway-crossing aircraft. To quantitatively evaluate the proportion of each part of the airflow in the inlet duct, especially the proportion of the internal airflow, mixed gas (oxygen, carbon dioxide, water, and nitrogen) was selected as the continuous fluid for calculation. The component transport in the numerical calculation was also considered. Additionally, in the setting of boundary

Table 1 Boundary-condition-setting parameters

Boundary position	Parameter settings	Component settings
Core nozzle entrance	$P_c^* = 163688$ Pa $T_c^* = 841.86$ K	$f_{O_2} = 15.63\%$, $f_{CO_2} = 3.47\%$ $f_{H_2O} = 3.47\%$, $f_{N_2} = 77.42\%$ $f_{O_{18}} = 0\%$, $f_{N_{15}} = 0\%$
Bypass nozzle entrance	$P_b^* = 176950$ Pa $T_b^* = 346.55$ K	$f_{O_2} = 21\%$, $f_{CO_2} = 0\%$ $f_{H_2O} = 0\%$, $f_{N_2} = 79\%$ $f_{O_{18}} = 0\%$, $f_{N_{15}} = 0\%$
Far-field entrance of the nozzle	$P_0^* = 101388$ Pa $T_0^* = 300$ K	$f_{O_2} = 0\%$, $f_{CO_2} = 0\%$ $f_{H_2O} = 0\%$, $f_{N_2} = 0\%$ $f_{O_{18}} = 21\%$, $f_{N_{15}} = 79\%$
Far-field exit of the nozzle	$P_b = 101325$ Pa	/
Exit of the inlet	$\dot{m} = 135.3$ kg/s	/
Far-field entrance of the inlet	Determined according to the cross-sectional parameters extracted from the nozzle calculation results	Determined according to the cross-sectional parameters extracted from the nozzle-calculation results
Far-field exit of the inlet	$P_b = 101325$ Pa	/

conditions, the gas molar composition of each boundary condition was set according to the actual operation situation. the content of each gas entering the inlet was quantitatively analyzed by component identification. To distinguish the gas discharged from the nozzle from the gas in the far field, the oxygen and nitrogen in the far field was replaced with isotopes of oxygen and nitrogen, respectively. Table 1 shows the parameter settings and component settings of each boundary condition. The total temperature and the total pressure at the core and bypass entrances of the nozzle were the parameters when the engine of the takeoff aircraft was in the takeoff condition. The flow rate at the exit of the air inlet was the flow rate of the runway-crossing aircraft's engine when it was in an idle state, which was about 35% of the flow rate under the takeoff condition. The far-field exit pressures at the nozzle and the inlet were atmospheric pressure. The total temperature and the total pressure at the far-field entrance of the nozzle were the total temperature and the total pressure when the airflow Ma=0.03. The far-field entrance parameters of the inlet were defined according to the cross-section parameters extracted from the nozzle calculation results. The molar composition of each gas at the core nozzle inlet was obtained through forming a mixture of jet fuel (C_8H_{18}) and air with a residual gas coefficient of 4, and then the composition of each gas was obtained through complete combustion (Shi et al., 2013). The molar compositions of gas at the bypass nozzle entrance and the far-field exit were air, with the difference being that the oxygen and nitrogen at the far-field entrance were isotopes of oxygen and nitrogen, respectively.

The nozzle calculation model was used to test the mesh independence. The aforementioned numerical

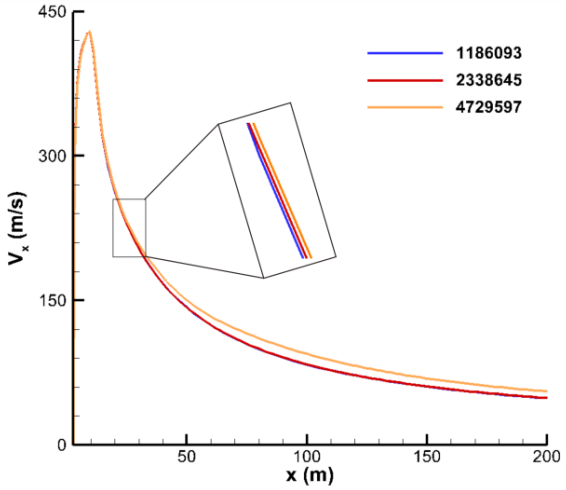

Fig. 7 Comparison of axial velocity distribution at the nozzle exit for different numbers of elements

simulation method was used to calculate the nozzle flow field with three different numbers of elements: 1,186,093, 2,338,645, and 4,729,597 elements. Figure 7 illustrations the comparison in velocity distribution in the x-direction on the outlet axis of the nozzle for these three different numbers of elements. It can be seen from the figure that the axial velocities at 2,338,645 and 4,729,597 elements largely coincided, while the result at 1,186,093 elements was very different from that of the other two, mainly in the area where x was greater than 50 m. Therefore, 2,338,645 elements were used to calculate the flow field of the nozzle. At this number of elements, meshing of the inlet model was performed, and the calculation model of the inlet had 3,392,324 elements. It

can also be seen from Fig. 6 that the velocity at the axis of the nozzle exit changed slowly after 100 m from the exit. Therefore, the aerodynamic parameters on the cross section of x=100 m were extracted from the nozzle flow field and assigned to the entrance boundary of the inlet.

It should be noted that the following assumptions are made in the numerical simulation process. (1) The gas is a perfect gas. (2) The inlet of the nozzle is uniform flow. (3) The gas components are obtained by complete combustion. (4) Both the take-off aircraft and the crossing-runway aircraft are stationary. (5) The far-field airflow velocity is almost zero. However, under actual conditions, the gas is not perfect gas. The airflow at the nozzle inlet is also not uniform. The combustion gas mixture cannot be completely burned in the combustion chamber. Both the take-off aircraft and the crossing-runway aircraft are in motion, and the airport is windy. These differences make the numerical simulation results different from the actual situations, mainly manifested in: (1) The flow field distribution of the jet is different; (2) The component proportion entering the rear engine is different. Therefore, it should be emphasized that this paper focuses on the discussion of research methods.

3. RESULTS AND DISCUSSION

3.1 Analysis of Impacts of the Jet from Takeoff Aircraft on the Inlet Distortion of Runway-Crossing Aircraft

Figure 8 shows the Mach number distribution for the global view on the symmetry plane of the nozzle calculation model and the local view of the nozzle area. It can be seen from the global view that the exhaust jet mainly affected the area near the nozzle axis. The farther away from the nozzle the location, the greater the impact range in the circumferential direction for the jet. From the local view of the nozzle area, it can be seen that the airflow gradually accelerated in the core and bypass nozzles, and the Mach number reached the maximum at the exit. Because the total pressure at the bypass nozzle entrance was higher than that of the core nozzle, the Mach number of the bypass nozzle exit was greater than that of the core nozzle. The presence of the tail cone created a low-energy recirculation zone behind the tail cone, and the corresponding Mach numbers of the airflow after this zone were all low. Owing to the different Mach numbers of the airflow at the exit of the bypass nozzle, the exit of the core nozzle, and behind the tail cone, there were three shears, namely between the far field and the bypass airflow, between the bypass airflow and the core airflow, and between the core airflow and the tail cone airflow. The velocity gradient in each shear layer was very large, and the viscous effect was significant. The airflow velocity of the core and bypass confinement decayed rapidly, and the airflow velocity of the core and bypass confinement tended to be consistent.

Figure 9 shows the distributions of the O_2 and O_{18} molar composition in the global view on the symmetry plane of the nozzle calculation model and in the local view of the nozzle area. It can be seen from the local view that the O_2 composition of the airflow in the bypass

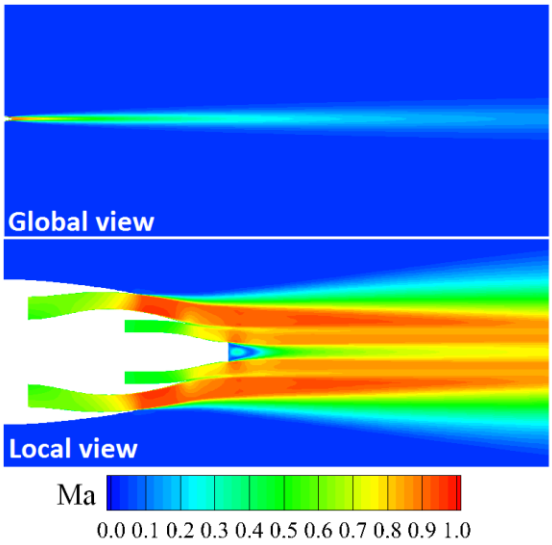

Fig. 8 Distribution of Mach numbers on the symmetry plane of the nozzle calculation model

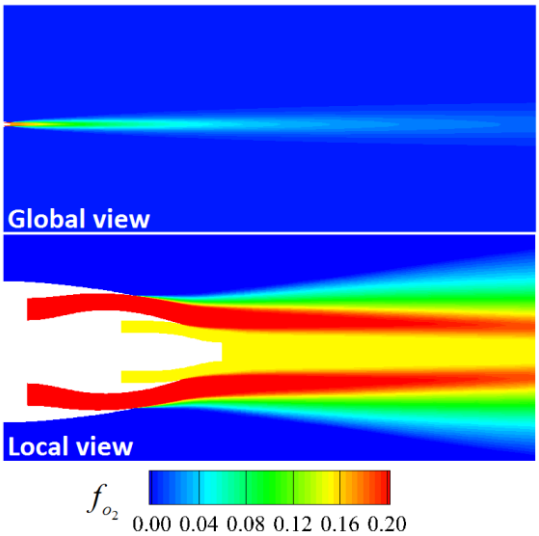

(a) Distribution of O_2 on the symmetry plane of the nozzle calculation model

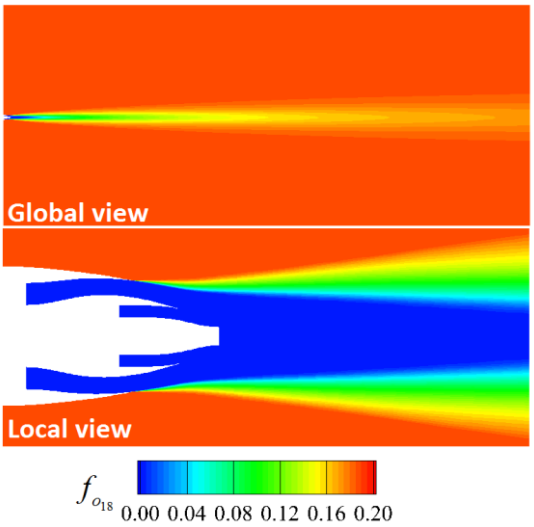

(b) Distribution of O_{18} on the symmetry plane of the nozzle calculation model

Fig. 9 Distribution of oxygen components on the symmetry plane of the nozzle calculation model

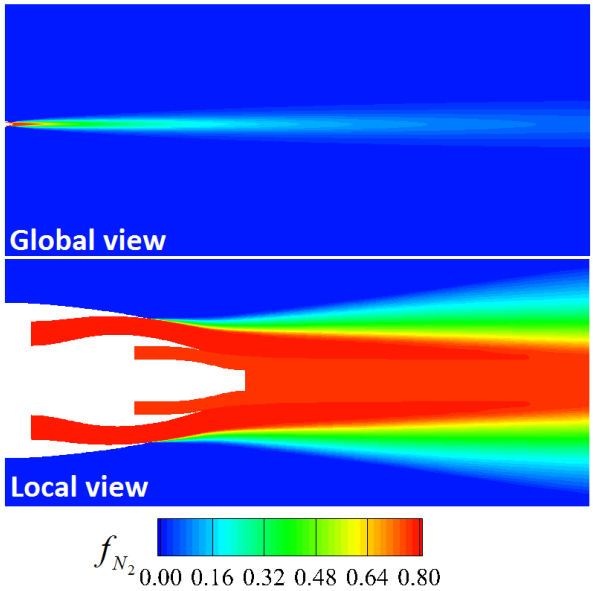

(a) Distribution of N_2 on the symmetry plane of the nozzle calculation model

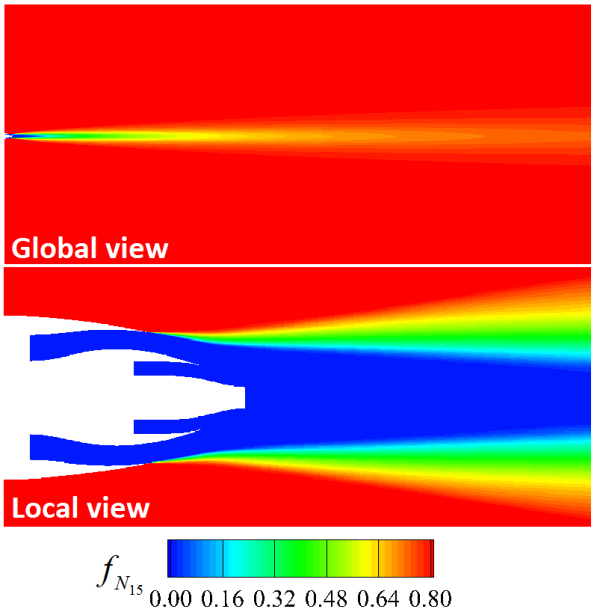

(b) Distribution of N_{15} on the symmetry plane of the nozzle calculation model

Fig. 10 Distribution of nitrogen on the symmetry plane of the nozzle calculation model

passage was 21% of the inlet setting, the O_2 composition of the airflow in the core passage was 15.63% of the inlet setting, and the O_2 composition of the far-field entrance airflow was zero. The airflows of these three different components were gradually mixed at the nozzle exit. As the airflow was moving backward, the O_2 composition in the jet area gradually decreased while the O_{18} composition gradually increased. The distributions of N_2 and N_{15} of the jet flow shown in Fig. 10 were similar to the distribution of oxygen; that is, the N_2 compositions gradually decreased in the jet region, while the N_{15} composition gradually increased. Figures 8 and 9 further show that the distributions of the other components (CO_2

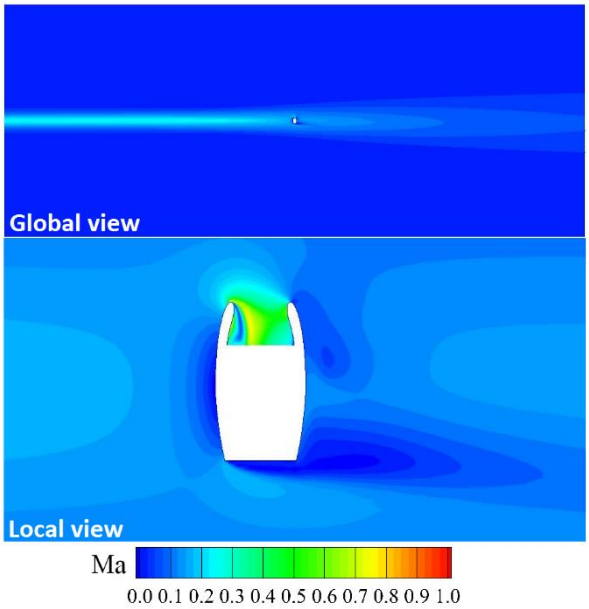

Fig. 11 Distribution of Mach numbers on the symmetry plane of the inlet calculation model

and H_2O, not presented here) were also similar to the distribution of oxygen, so this is not further described here.

Figure 11 shows the Mach number distributions at the global view on the symmetry plane of the inlet calculation model and at the local view of the inlet area. The boundary condition of the far-field entrance of the inlet was extracted from the cross section of the tail nozzle flow field at x=100 m, and the distance between the inlet and its far-field entrance was 150 m. This operating condition simulated the situation where the nozzle was 250 m away from the inlet. It can be seen from the global view that in the area after x=100 m, the Mach number distribution of the inlet was basically consistent with the Mach number distribution of the nozzle. It can be seen from the local view that the jet had formed a large crosswind condition on the inlet, which created serious airflow separation inside the lip near the nozzle side, reducing the recovery coefficient of the total pressure of the gas entering the engine and causing an extremely uneven airflow distribution in the engine passage. At the same time, owing to the rotation flow, flow separation occurred on the outer side of the lip far away from the nozzle and at the tail of the engine, causing an increase in the external resistance of the engine. This study mainly focused on the effects of the jet from the aircraft in front on the inlet distortion of the aircraft behind. The distributions of the total pressure at the inlet exit under different conditions are given later in this paper.

Figure 12 illustrates the distribution of the O_2 molar composition from the global view on the symmetry plane of the inlet model from the local view of the inlet area. Similar to the aforementioned inlet Mach number distribution, in the region after x=100 m, the distribution of O_2 in the inlet was basically consistent with the distribution of O_2 in the nozzle, further verifying the

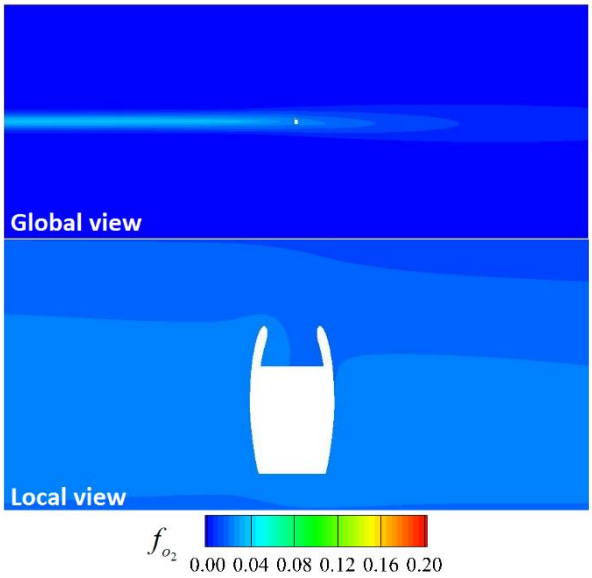

Fig. 12 Distribution of oxygen components on the symmetry plane of the inlet calculation model

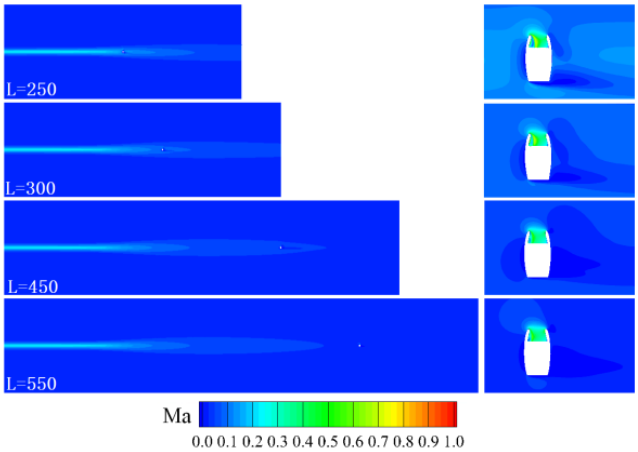

Fig. 13 Distribution of Mach numbers on the symmetry plane of the inlet calculation model at different jet distances

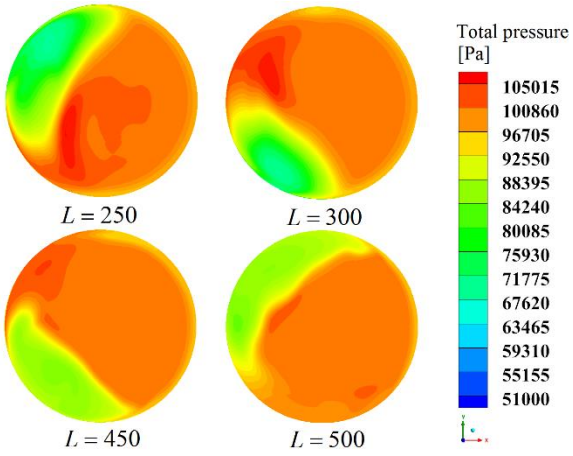

Fig. 14 Distribution of total pressure on the exit cross section of the inlet at different jet distances

accuracy of the method that extracts the boundary from the nozzle flow field and assigns it to the value at the inlet entrance. It can be seen from the local view that, owing to the large flow separation in the inlet passage, the flow distribution was extremely uneven, leading to an uneven distribution of the airflow components. The uneven distribution of the flow field and the uneven distribution of the airflow components can cause inlet distortion, thereby affecting the operating stability of the compressor and the combustion chamber.

3.2 Analysis of Impacts of Jet from Takeoff Aircraft on the Inlet Distortion of Runway-Crossing Aircraft at Different Distances

The aforementioned simulation was conducted with the flow at the inlet exit at 135.3 kg/s and the distance between the inlet and the nozzle at 250 m. To analyze the jet at different distances between the inlet and the nozzle, based on the above simulation, 60-m-wide rectangular far-field areas at lengths of 50 m, 200 m, and 300 m were set up, and meshing was performed according to the mesh density of the inlet. In the numerical calculation, first, the three far-field meshes were joined with the far-field meshes of the inlet to form a longer far-field area of the inlet. Then, aerodynamic parameters on the cross section at x=100 m extracted from the tail nozzle flow field were assigned to the new far-field entrance of the inlet. Finally, the inlet flow fields at these three different distances—namely, 300 m (corresponding to the 50-m rectangular far-field area), 450 m (corresponding to the 200-m rectangular far-field area), and 550 m (corresponding to the 300-m rectangular far-field area) were calculated.

Figure 13 shows the distribution of Mach numbers from the global view on the symmetry plane of the inlet and the local view of the inlet area at different distances. It can be seen that as the distance between the inlet and the nozzle increased, the effects of the jet on the inlet gradually decreased. The inlet faced a relatively large crosswind environment at small distances, and there were relatively severe flow separations on the inner side of the lip of the air inlet near the nozzle side, the outer side of the lip of the inlet away from the nozzle, and the tail of the engine. As the distance increased, the speed of the crosswind decreased, and the separation areas at these three locations were gradually reduced.

Figure 14 illustrates the distribution of total pressure on the cross section of the exit of each inlet at different distances. The low-pressure area in the figure was caused by the flow separation inside the lip. As the distance increased, the locations of the separation areas in the circumferential direction changed accordingly, and at the same time, the minimum pressure on the cross section gradually increased. Owing to the different distances, the total pressure, velocity, and static pressure of the airflow entering the inlet were different. Thus, the maximum pressure on the cross section of the exit of the inlet was also different. To quantitatively describe the inlet distortion caused by the jet at different distances, the distortion index given by Eq. (6) was used to characterize the uniformity of the flow field.

Table 2 Distortion index at the exit of the outlet at different distances

Distances (m)	$\bar{D}$	Mass-weighted average molar composition of each component					
		f_{CO_2}	f_{H_2O}	f_{N_2}	f_{O_2}	$f_{N_{15}}$	$f_{O_{18}}$
250	0.337	0.047%	0.047%	7.706%	1.981%	73.193%	17.026%
300	0.326	0.028%	0.028%	4.610%	1.186%	76.378%	17.771%
450	0.210	0.012%	0.012%	1.925%	0.495%	79.140%	18.417%
550	0.220	0.009%	0.009%	1.408%	0.362%	79.671%	18.542%

$$\bar{D} = \frac{p^*_{\max} - p^*_{\min}}{\overline{p^*}} \tag{6}$$

where $p^*_{\max}$, $p^*_{\min}$, and $\overline{p^*}$ are the maximum, minimum, and mass-weighted average of the total air pressure on the cross section of the exit of the inlet, respectively.

Table 2 shows the total pressure distortion index and the mass-weighted average of each component on the cross sections of the inlet exits at different distances. It can be seen that as the distance between the inlet and the nozzle increased, the total pressure distortion index at the exit of the inlet decreased. This is because the larger the distance, the lower the incoming flow velocity into the inlet, and the less flow separation loss inside the lip. At the same time, with the increase of the distance, the contents of the components (including CO_2, H_2O, N_2, and O_2) of the airflow entering the inlet from the engine jet decreased, while the contents of the components (including N_{15} and O_{18}) of the airflow entering the inlet from the far field increased. This is because as the distance increased, the jet was diluted by the far-field airflow, and thus, the jet entering the inlet decreased, and the far-field flow increased.

In addition, Table 2 quantitatively demonstrates that even at the minimum distance (i.e., 250 m), the CO_2 and H_2O entering the inlet only accounted for 0.047% each. The airflow components entering the inlet were mostly nitrogen and oxygen. Therefore, when studying the effects of the aircraft in front on the aircraft behind, the impacts of the components of the jet on the inlet can be ignored, but the inlet distortion caused by the jet in the crosswind environment cannot be ignored.

3.3 Analysis of Impacts of Jet from Takeoff Aircraft on the Inlet Distortion of Runway-Crossing Aircraft at Different Inlet Exit Flow Rates

Given that the rotating speed of the engine at an idle state is 20%–35% of the maximum rotating speed, the previous section discussed the simulation of the situation for the 35% operating conditions. To analyze the jet with different flow rates at the exit of the inlet, the calculations were performed for the flow rates at the exit of the inlet being 77.3 kg/s, 96.6 kg/s, and 115.9 kg/s, corresponding to 20%, 25%, and 30% operating speed conditions, respectively. The distance between the nozzle and the inlet was 450 m for these cases.

Figure 15 shows the distribution of the Mach number in the local view of the inlet area for different exit flow rates. It can be seen that owing to the jet flow distance being the same, the Mach number distributions of the incoming flow in these four operating conditions

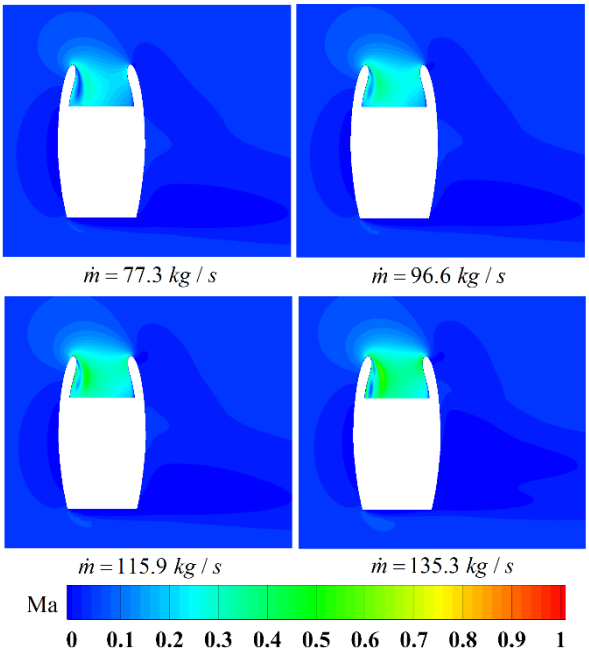

Fig. 15 Distribution of Mach numbers on the symmetry plane of the calculation model at different flow rates at the exit of the inlet

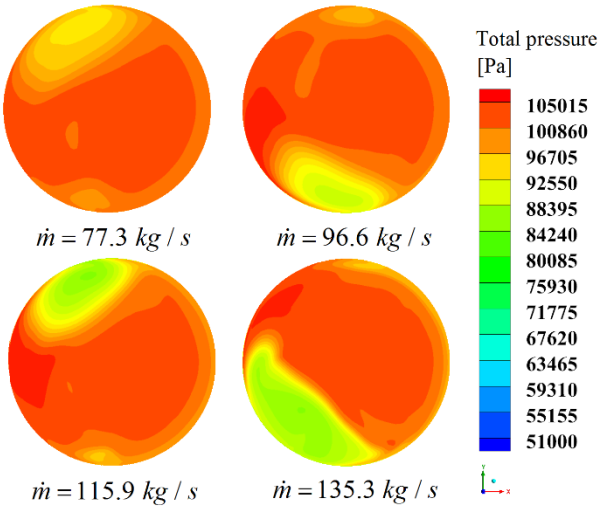

Fig. 16 Distribution of total pressure on the cross section of the exit of the inlet at different exit flow rates

were essentially the same. The difference was that as the flow rate at the exit of the inlet increased, the velocity of the airflow entering the inlet became larger and the corresponding flow loss became larger. Figure 16 shows

Table 3 Parameters at the exit of the inlet for different outlet flow rates

Exit flow rate (kg/s)	Mass-weighted average total pressure (Pa)	Mass-weighted average molar composition of each components					
		f_{CO_2}	f_{H_2O}	f_{N_2}	f_{O_2}	$f_{N_{15}}$	$f_{O_{18}}$
77.3	100971	0.011708%	0.011705%	1.92706%	0.495686%	79.1370%	18.4168%
96.6	100566	0.011705%	0.011701%	1.92654%	0.495553%	79.1376%	18.4169%
115.9	100267	0.011693%	0.01169%	1.92464%	0.495064%	79.1395%	18.4174%
135.3	100171	0.011693%	0.011689%	1.92451%	0.495037%	79.1396%	18.4174%

the total pressure distribution at the exit of the inlet under these four working conditions. As the flow at the exit increased, the position of the separation zone in the circumferential direction changed accordingly, and at the same time, the minimum pressure value on the cross section became gradually smaller; that is, the flow loss increased.

Table 3 shows the mass-weighted average total pressure and components on the cross sections at the exit of the inlet at different exit flow rates. It can be seen that with the increase of the exit flow rate of the inlet, the total pressure at the exit of the inlet decreased. This is because the greater the flow rate, the greater the velocity of the airflow entering the inlet, and the greater the flow separation loss occurring inside the lip. At the same time, for the different exit flow rates, the content of each component of the airflow entering the inlet was the same, and the difference in the flow rate had little effect on the components. This is because at the same distance, the distribution of the incoming flow in the inlet was consistent, and only the airflow velocities were different. Therefore, when studying the impacts of the jet from the aircraft in front on the aircraft behind, only the maximum idle engine speed condition needed to be considered.

4. CONCLUSION

This paper discussed the effects of the jet from an aircraft in front on the air inlet of an aircraft behind crossing a runway, mainly focusing on the discussion of research methods. The following conclusions can be drawn:

(1) The multi-step calculation method, in which the parameters from the nozzle flow field are extracted and assigned to the entrance boundary of the inlet to facilitate the structured meshing of the complex calculation model of the nozzle and the inlet, reduces the amount of calculation, saves calculation time, and achieves reliable calculation results. The method of component and isotope identification can be used to quantitatively analyze the content of each component of the flows entering the inlet from the nozzle and its far field so that the effects of the jet components can be clearly and accurately evaluated;

(2) The large crosswind conditions formed by the jet on the inlet lead to severe flow separation inside the inlet, leading to increased flow loss and uneven flow distribution in the inlet. At the same distance between the nozzle and the inlet, as the exit flow rate of the inlet increases, the total outlet pressure decreases, but the components of the airflow entering the inlet are essentially the same. At the same flow rate at the exit of the inlet, as the distance between the nozzle and the inlet increases, the distortion index of the total pressure at the exit of the inlet decreases, and the content of each component of the airflow entering the inlet from the engine jet decreases, while the content of each component of the airflow entering the inlet from the far field increases;

(3) The composition of the airflow entering the inlet is identified by its components and isotopes. It is found that even at the minimum distance, only a small portion of the exhaust gas (carbon dioxide and water) in the jet enters the inlet (less than 0.05%), and the main components of the airflow entering the inlet are still oxygen and nitrogen. Along with the calculation results under different flow rates, it can be determined that when studying the effects of the aircraft in front on the aircraft behind, only the maximum idle engine speed condition needs to be considered, and the effects of the jet components on the inlet can be ignored;

(4) The inlet distortion caused by the jet is relatively severe in the crosswind environment. The engine of the aircraft behind is already in an idle state, and its compressor is prone to surging. Therefore, future studies should focus on the effects of the inlet distortion on the stability of the compressor and the combustion chamber to provide appropriate suggestions for pilots to handle their engines properly in the mode of runway crossing behind a takeoff aircraft.

ACKNOWLEDGMENTS

The authors express their gratitude for the financial support of the National Natural Science Foundation of China (No. 52305170), the Sichuan Natural Science Foundation Project Youth Science Foundation Project (No. 2022NSFSC1894, No. 2023NSFSC0837, and No. 2022NSFSC1885), and the Fundamental Research Funds for the Central Universities Research Fund (No. 24CAFUC03032).

CONFLICT OF INTEREST

The authors state that there are no conflicts to disclose.

AUTHORS CONTRIBUTION

Xiao-lin Sun: methodology, investigation, validation, writing – original draft. **Wen Cheng:** data curation. **Yao-ming Fu**: supervision. **Xin He:** validation.

Ya-qing Chen: formal analysis. **Shan Ma:** writing-review-editing.

REFERENCES

Chen, Y., & Zhang, X. (2018). A preliminary study on schemes on crossing runway behind takeoff aircraft at the Chongqing Jiangbei airport. *Journal of Civil Aviation*, *2*(4), 25-30. https://doi.org/CNKI:SUN:MHXE.0.2018-04-007

Chen, Y., Hu, D., & Hou, B. (2019). Taxiing route planning of aircraft based on rear runway crossing way of take-off aircraft. *Aeronautical Computing Technique*, *49*(2), 11-14. https://doi.org/10.3969/j.issn.1671-654X.2019.02.003

Chen, Y., Liu, C., & He, X. (2021a). Influence of natural wind on jet distance of engine. *Science Technology and Engineering*, *21*(32), 13986-06. https://doi.org/10.3969/j.issn.1671-1815.2021.32.051

Chen, Y., Zhang, Z., & Huang, C. (2021b). Simulation optimization of AnyLogic taxiing behind based on conflict avoidance. *Aeronautical Computing Technique*, *51*(03), 5-9. https://doi.org/10.3969/j.issn.1671-654X.2021.03.002

Donald, S. M., & Matt, A. W. (2005). *Effects of inlet distortion on the stability of an advanced military swept fan stage with casing treatment.* ASME Turbo Expo 2005: Turbine Technical Conference and Exposition, GT-2005-68693. https://doi.org/10.1115/GT2005-68693

Guo, D. (2023). *Study on jet influence distance of takeoff aircraft based on CFD*. Civil Aviation Flight University of China. https://doi.org/10.27722/d.cnki.gzgmh.2023.000056

He, X., & Zhang, F. (2019a). Efficiency comparison between front and rear crossing in Chongqing Jiangbei airport based on AnyLogic. *Aeronautical Computing Technique*, *49*(4), 39-43. https://doi.org/10.3969/j.issn.1671-654X.2019.04.010

He, X., & Zhang, F. (2019b). Research on the way of taking off the runway on the back side of take-off aircraft. *Value Engineering*, *38*(20), 195-197. https://doi.org/10.14018/j.cnki.cn13-1085/n.2019.20.062

He, X., Hu, D., Chen, Y., & Zhang, Z. (2020a). Numerical simulation of jet flow of take-off aircraft based on rear runway crossing way of take-off Aircraft. *Aeronautical Computing Technique*, *50*(6), 5-8. https://doi.org/10.3969/j.issn.1671-654X.2020.06.002

He, X., Li, L., & Hu, D. (2021). Research on anti-crosswind capability of rear aircraft under mode of back crossing of takeoff aircraft. *Aeronautical Computing Technique*, *51*(2), 5-9. https://doi.org/10.3969/j.issn.1671-654X.2021.02.002

He, X., Zhang, Z., Chen, Y., & Zhang, F. (2020b). Analysis of taxiing efficiency in the rear crossing mode of take-off aircraft. *Science Technology and Engineering*, *20*(24), 10079-10087. https://doi.org/10.3969/j.issn.1671-1815.2020.24.057

Hu, D. (2020). *Research on safety intervals of runway crossing at the back of take-off aircraft*. Civil Aviation Flight University of China. https://cdmd.cnki.com.cn/Article/CDMD-10624-1020041467.htm

International Civil Aviation Organization (2010). *Tacking the global issue of runway safety*. The assembly-37th session technical commission, A37-WP/68. https://www.icao.int/Meetings/AMC/Assembly37/Working%20Papers%20by%20Number/wp068_en.pdf

Jiang, H. B., Lu, Y. J., Yuan, W., & Li, Q. S. (2009). *Experimental investigation of the influence of inlet distortion on the stall inception in a low speed axial compressor*. ASME Turbo Expo 2009: Turbine Technical Conference and Exposition, GT-2009-59139. https://doi.org/10.1115/GT2009-59139

Lu, Q., & Yu, T. (2011). Crossing runways in a safe and efficient way in multi-runway operation. *Safety & Security*, *06*, 59-62. https://doi.org/CNKI:SUN:MHJJ.0.2011-06-021

Ren, W., & W. L. I. (2015). Impact of runway crossing point settings to closely spaced parallel runway capacity. *Aeronautical Computing Technique*, *45*(4), 49-56. https://doi.org/10.3969/j.issn.1671-654X.2015.04.013

Ross, M. H., Oliva, A., & Fidalgo, V. J. (2018). *Experimental and numerical characterization of transonic compressor subjected to inlet distortion.* ASME Turbo Expo 2018: Turbine Technical Conference and Exposition 2018, GT-2018-76653. https://doi.org/10.1115/GT2018-76653

Shi, X., Ji, H., Si, R., & Liao, H. (2013). Comparative investigation of infrared radiation characteristics of asymmetrical individual and mixing exhaust systems in a turbofan engine. *Journal of Aerospace Power*, *28*(8), 1702-1710.

Society of Automotive Engineers. (1991). *A Current Assessment of the Inlet/Engine Temperature Distortion Problem*. Standard number: ARD-50015. https://www.intertekinform.com/en-us/standards/sae-ard-50015-1991-1018446_saig_sae_sae_2370610/

Society of Automotive Engineers (2023). Inlet Total-Pressure Distortion Considerations For Gas-Turbine Engines. Standard number: AIR-1419D. https://www.intertekinform.com/en-us/standards/sae-air1419d-2023-1018101_saig_sae_sae_3330752

Thomas, P., & Leonhard, F. (2002). *Effects of co- and counter-rotating inlet distortions on a 5-stage HP-compressor*. ASME Turbo Expo 2002: Turbine Technical Conference and Exposition, GT-2002-30395. https://doi.org/10.1115/GT2002-30395

Wang, Q. (2023). *Research on taxiing stability of aircraft running behind takeoff point*. Civil Aviation Flight University of China. https://doi.org/10.27722/d.cnki.gzgmh.2023.000090

Yan, W., Hu, J., & Zhang, H. (2014). Effects of complicated rotating inlet distortion on compressor aerodynamic stability. *50th AIAA/ASME/SAE/ASEE Joint Propulsion Conference*, AIAA-2014-3732. https://doi.org/10.1115/GT2017-63369

Zhang, F. (2019*). Research on taxiway optimization based on the runway through behind the take-off point.* Civil Aviation Flight University of China. https://cdmd.cnki.com.cn/Article/CDMD-10624-1019128446.htm.

Zhang, Y., Rudis, R. P., Wang, F. Y., Spitzer, E. (2016). Simulation of jet blast effect on landing aircraft. *Air Traffic Control Quarterly*, *9*(3), 211-227. https://doi.org/10.2514/atcq.9.3.211

Zhang, Z. (2021). *Research on taxiing efficiency of multi-runway airport based on crossing runway behind take-off aircraft*. Civil Aviation Flight University of China. https://cdmd.cnki.com.cn/Article/CDMD-10624-1020041467.htm